



## Abstract

Avalanches can exhibit many different flow regimes from powder clouds to slush flows. Flow regimes are largely controlled by the properties of the snow released and entrained along the path. Recent investigations showed the temperature of the moving snow to be one of the most important factors controlling the mobility of the flow. The temperature of an avalanche is determined by the temperature of the released and entrained snow but also increases by frictional and collisional processes with time. For three artificially released avalanches, we conducted snow profiles along the avalanche track and in the deposition area, which allowed quantifying the temperature of the eroded snow layers. Infrared radiation thermography (IRT) was used to assess the surface temperature before, during and just after the avalanche with high spatial resolution. This data set allowed to calculate the thermal balance, from release to deposition, and to discuss the magnitudes of different sources of thermal energy of the avalanches. We could confirm that, for the investigated dry avalanches, the thermal energy increase due to friction was mainly depending on the elevation drop of the avalanche with a warming of approximately  $0.5^{\circ}\text{C}$  per 100 height meters. Contrary, warming due to entrainment was very specific to the individual avalanche and depended on the temperature of the snow along the path and the erosion depth ranging from nearly no warming to a maximum observed warming of  $1^{\circ}\text{C}$ . Furthermore, we could observe the warmest temperatures are located in the deposits of the dense core. Future research directions, especially for the application of IRT, in the field of thermal investigations in avalanche dynamics are discussed.

## 1 Introduction

Avalanches can exhibit many different flow regimes (Gauer et al., 2008) depending on (1) the released and entrained amount of snow, (2) the properties of the snow and (3) the topography (slope, curvature) (Naaïm et al., 2013). Studies showed that

TCD

8, 5793–5824, 2014

## Thermal energy in dry snow avalanches

W. Steinkogler et al.

Title Page

Abstract

Introduction

Conclusions

References

Tables

Figures



Back

Close

Full Screen / Esc

Printer-friendly Version

Interactive Discussion



## Thermal energy in dry snow avalanches

W. Steinkogler et al.

Title Page

Abstract

Introduction

Conclusions

References

Tables

Figures



Back

Close

Full Screen / Esc

Printer-friendly Version

Interactive Discussion



avalanches can increase their mass due to entrainment by multiple factors (Sovilla et al., 2007; Bates et al., 2014) which in turn influences the run-out distance. Even though important, the amount of snow entrained is not the main controlling factor that determines the flow form of the avalanche (Bartelt et al., 2012). The flow regimes and in turn mobility are strongly influenced by the properties of the entrained snow (Steinkogler et al., 2013). Data on front velocities, run out, flow regimes and powder clouds revealed that different avalanches can form with similar release conditions and on the same avalanche path depending on the inherent snow cover properties.

Recently, it has been shown that snow temperature inside an avalanche can significantly change its flow dynamics (Naaïm et al., 2013; Steinkogler et al., 2013), mainly by changing the granular structure of the flow (Steinkogler et al., 2014). Laboratory studies on the granulation of snow showed a distinct dependency on snow temperatures with a fundamental change in snow structure at a threshold of  $-1^{\circ}\text{C}$ . Therefore, significant changes in flow dynamics can be expected with relatively small changes in temperature around this threshold.

Measuring temperature inside a flowing avalanche or in its deposit with traditional methods has proven to be difficult due to technical constraints or because measurements can not be conducted due to safety reasons. In addition to manual snow profiles we therefore investigate the application potential of infrared radiation thermography (IRT) technologies. IRT is a non-contact, non-intrusive technique, which enables us to see surface temperature in a visible image. Meola and Carlomagno (2004) give an overview on existing work and describe the most relevant industrial and research applications of IRT.

The emissivity of a surface is a function of many factors, including water content, chemical composition, structure and roughness (Snyder et al., 1998) as well as the viewing angle between observer and measurement object. Even though many technical challenges and shortcomings of IRT are known, possible applications on the field of snow science have recently been discussed (Shea and Jamieson, 2011). Shea et al. (2012) and Schirmer and Jamieson (2014) applied IRT to measure spatial snow

## Thermal energy in dry snow avalanches

W. Steinkogler et al.

Title Page

Abstract

Introduction

Conclusions

References

Tables

Figures



Back

Close

Full Screen / Esc

Printer-friendly Version

Interactive Discussion



surface temperatures on snow pit walls. It was found that fast and large temperature changes resulting from surface energy balance processes must be expected (Schirmer and Jamieson, 2014). These energy balance processes between air and snow are particularly important during windy conditions, clear skies and large temperature differences between air and snow. These findings indicate that measuring the snow surface temperature of avalanche deposits or erosion layers along the track must be carried out as fast as possible. IRT can therefore be seen as a useful qualitative tool for snow applications whose quantitative operation still needs further verification.

The aim of this study is to identify the spatial temperature distribution in an avalanche and to quantify potential sources of thermal energy in an order of magnitude estimation. This is achieved by field measurements and the application of an IRT camera. Furthermore, the acquired IRT videos allow to observe the avalanche phenomenon from a mainly qualitative but nevertheless unique point of view.

## 2 Methods and data

### 2.1 The Flüelapass field site

Multiple dry avalanches were artificially released during winters 2012–2013 and 2013–2014 at the Flüelapass field site above Davos (Switzerland). Here we will discuss three avalanches, #1 (23 January 2013), #2 (5 February 2013) and #3 (31 January 2014), out of this data base (Fig. 1).

The avalanche path is a north-east facing slope covering 600 vertical meters. Deposits of larger avalanches typically reach a lake located at 2374 m a.s.l. at the bottom of the slope (Fig. 2). Observations and remote measurements can safely be conducted from the road at the pass. The slope angle ranges from 50° in the rock face in the upper part to 20° at the beginning of the run-out zone with an average of 30° of the open slope around 2600 m a.s.l.

## 2.2 Snow profiles

To assess the properties of the released and entrained snow, manual snow profiles according to Fierz et al. (2009) were conducted in the release zone ( $P_{\text{release}}$ ), i.e. just below the rock face, along the track ( $P_{\text{track}}$ ), in the deposition zone ( $P_{\text{depo}}$ ) and in the undisturbed snow cover in the run out zone ( $P_{\text{runout}}$ ) (Fig. 2). The profile location of the initially released cornice is referred to as  $P_{\text{cornice}}$ . In combination with release and erosion depths, the acquired snow profiles allowed to identify which layers were entrained into the avalanche.

All profiles were conducted as fast as possible after the avalanche stopped. Yet, especially for the profiles in the release area and the track, it took around 30 min to reach the profile locations. The temperature measurements close to the surface must therefore be interpreted carefully due to a rapid adaptation to the ambient conditions.

## 2.3 Lateral temperature profiles

In addition to the regular snow profiles, trenches were dug in the deposition zone and modified avalanche probes were used to measure lateral temperature gradients. The modified temperature probes (BTS) are regular avalanche probes for which the tip was replaced by a thermistor. BTS probes are usually used for permafrost applications (Lewkowicz and Ednie, 2004; Brenning et al., 2005) to measure the temperature at the interface between soil and snow. Their application allowed to measure the temperature of snow layers without exposing them to the ambient air temperature. As for the thermometers used for regular snow profiles (Sect. 2.2) they measure the snow temperature with an accuracy of  $\pm 0.1^\circ\text{C}$ . As for the regular snow profiles the upper most layers need to be interpreted carefully in this investigation due to an expected change in temperature over time.

The lateral temperature measurements were conducted to the left and right side of snow profile  $P_{\text{depo}}$ , which was situated in the center of the deposition zone (Fig. 2).

TCD

8, 5793–5824, 2014

## Thermal energy in dry snow avalanches

W. Steinkogler et al.

Title Page

Abstract

Introduction

Conclusions

References

Tables

Figures

◀

▶

◀

▶

Back

Close

Full Screen / Esc

Printer-friendly Version

Interactive Discussion



## 2.4 Infrared radiation thermography (IRT) camera

The snow temperature measurements acquired from profiles were supplemented with an infrared radiation thermography (IRT) camera which allowed to record snow surface temperatures before, during and after the avalanche (Figs. 3 and 5). Time-lapse measurements after the avalanche stopped allowed to follow the temporal evolution of surface temperatures (Fig. 4) and videos of the moving avalanche provided a qualitative yet illustrative point of view (provided as Supplement).

We used an InfraTec VarioCAM hr 384 sl and a VarioCAM HD 980 s that both operate in the long wave infrared spectral range (LWIR) covering 7.5 to 14  $\mu\text{m}$ . According to the manufacturer the cameras measure with an absolute accuracy of  $\pm 1.5^\circ\text{C}$  and a resolution of  $0.05^\circ\text{C}$ . The measurements were either conducted with a 15 mm or a 30 mm lens.

Even though in our study we use the IRT measurements mainly in a qualitative way, a basic verification was conducted. The snow surface temperatures recorded with the IRT camera (solid lines in Fig. 4) were compared to manually measured snow surface temperatures (dots in Fig. 4) at the corresponding snow profile locations (Fig. 2). The snow surface temperatures of the release ( $T_{\text{IRT}_{\text{release}}}$ ) was compared to the corresponding layer in the snow profile in the undisturbed snow ( $T_{\text{P}_{\text{release}}}$  at 0 min) and measured surface temperatures with a digital thermometer ( $T_{\text{P}_{\text{release}}}$  at 45 min). The same was conducted for the surface temperature along the erosion layer in the avalanche path ( $T_{\text{P}_{\text{track}}}$ ). Both measurements are in fairly good agreement with an absolute difference of about  $\pm 1^\circ\text{C}$ .

## 2.5 Terrestrial laser scan (TLS)

A terrestrial laser scanner (Riegli LPM-321) was operated from the Flüelapass road (Fig. 2) to acquire digital surface models before and after the avalanche releases. The measurements facilitated the calculation of the release and erosion depths along the path. A complete set of terrestrial laser scans is available for avalanche #3 only. For

Title Page

Abstract

Introduction

Conclusions

References

Tables

Figures



Back

Close

Full Screen / Esc

Printer-friendly Version

Interactive Discussion



avalanche #2 the scan before the avalanche is only available for the release zone (Fig. 2). No information from terrestrial laser scanning was available for avalanche #1.

### 3 Investigated avalanches

This section summarizes the key characteristics and available data (Table 1) of the avalanches. All avalanches were released after a snow storm by triggering the cornices at the ridge at 2900 m a.s.l. with explosives. Therefore, most of the released snow was new snow. Yet, two of the avalanches, avalanche #2 and #3 (Fig. 1b and c), entrained significant amounts of snow from deeper layers due to a step-down, i.e. a secondary release to a deeper weak layer, below the rock face. Since the main mass contribution can be assumed to be defined by the secondary releases below the rock face and the entrainment along the path, we focused our investigations on these snow masses. Mass contributions by the cornices are usually relatively small compared to entrained snow on the open slope below. Furthermore, entrainment of snow in the gullies of the rock face is not assumed to contribute a significant amount since regularly occurring (small) avalanches and slides continuously erode the snow cover. In this study we use the word release to refer to profile locations at the secondary release below the rock face (Fig. 2).

#### Avalanche #1a and #1b (23 January 2013)

In the days previous to the avalanche experiment 10 cm of new snow were recorded and snow drift accumulations formed due to strong southerly winds. The national avalanche bulletin reported a moderate avalanche danger (level 2) and identified the fresh snow drift accumulations as the main danger. During the experiment clear sky conditions prevailed and the automatic weather station (AWS) at the Flüelapass (FLU2) measured an air temperature of  $-10^{\circ}\text{C}$ . Multiple charges were exploded on the ridge to the lookers-left (South) of the summit resulting in two independent small powder

## Thermal energy in dry snow avalanches

W. Steinkogler et al.

Title Page

Abstract

Introduction

Conclusions

References

Tables

Figures



Back

Close

Full Screen / Esc

Printer-friendly Version

Interactive Discussion



5 avalanches which followed the gullies (Figs. 1a and 3). Due to the relatively small re-  
lease mass and no significant entrainment both avalanches, #1a and #1b, stopped half  
way down the open slope. Even though the avalanches were small and a full data set  
of field measurements is not available, they are retained in this study since they pro-  
vide good quality IRT data (Fig. 3). We excluded the snow profile measurements from  
the analysis since the erosion and deposition depths were very small, around 0.1 m,  
and the manual measurements were conducted more than 1 h after the release. The  
deposition zone was not accessible before due to safety reasons. The TLS could not  
be completed due to technical problems.

### 10 **Avalanche #2 (25 February 2013)**

20 cm of fresh snow that covered older snow drift accumulations resulted in a consid-  
erable (level 3) avalanche danger. Furthermore, the bulletin noted that avalanches in  
isolated cases could be released deeper within the snowpack. The AWS at Flüelapass  
measured  $-12^{\circ}\text{C}$  and a partly cloudy sky prevailed during the experiment.

15 Explosions along the ridge and to the lookers-left (South) side of the summit only  
produced small avalanches that stopped shortly below the rock face. A single explosion  
that triggered the cornice to the right side of the summit caused another small powder  
avalanche that followed the gully and triggered a secondary release at the start of the  
open slope (Fig. 1b). Even though the avalanche almost stopped after entering the  
open slope, the additional mass which was entrained resulted in an re-acceleration  
20 resulting in a long running medium-sized avalanche (deposition mass 2357 t) which  
only stopped in the flat part close to the lake.

### **Avalanche #3 (31 January 2014)**

25 Multiple consecutive smaller snowfalls and strong southerly winds created snow accu-  
mulations close to ridges. The national avalanche bulletin issued a considerable (level  
3) danger level and that the weak old snowpack could cause avalanches to be released

## Thermal energy in dry snow avalanches

W. Steinkogler et al.

Title Page

Abstract

Introduction

Conclusions

References

Tables

Figures



Back

Close

Full Screen / Esc

Printer-friendly Version

Interactive Discussion



in near-ground layers. Moderate winds with gusts up to  $60 \text{ km h}^{-1}$  from the South and cloudy to overcast conditions prevailed during the experiment. The automatic weather station FLU2 recorded  $-6^\circ\text{C}$  with steadily increasing temperatures during the experiment.

Two small spontaneous avalanches already released before the experiment. Initial bombing of the main gully and to the lookers-left (South) of the summit did not produce any significant avalanches. Yet, the bombing of the cornice to the lookers-right (North) of the summit resulted in a small powder avalanche which triggered a second slide at the lower end of the rock face (similar to avalanche #2). Consequently a significant amount of snow was eroded and resulted in a medium-sized avalanche (deposition mass 2120t) that stopped in the flat run out zone (Fig. 1c). The secondary release nearly entrained all layers to the bottom of the snowpack (1.6 m). For avalanche #3 snow temperature measurements were also available for the cornice at the ridge.

## 4 Results

Based on these measurements we present observed temperature distributions during the avalanche motion as well as at the surface and inside the deposition zone (Sect. 4.1). In a second step potential sources of thermal energy are identified and quantified (Sect. 4.2).

### 4.1 Temperature distribution

#### 4.1.1 Avalanches in motion

The use of the IRT camera gave very interesting qualitative insights into the temperature behavior of a moving avalanche (Fig. 3 and 5). Especially plume formation, entrainment of warmer snow and the stopping of the avalanche as the powder cloud starved and drifted aside could be very well observed (see Supplement for the videos).

TCD

8, 5793–5824, 2014

## Thermal energy in dry snow avalanches

W. Steinkogler et al.

Title Page

Abstract

Introduction

Conclusions

References

Tables

Figures



Back

Close

Full Screen / Esc

Printer-friendly Version

Interactive Discussion



## Thermal energy in dry snow avalanches

W. Steinkogler et al.

Title Page

Abstract

Introduction

Conclusions

References

Tables

Figures



Back

Close

Full Screen / Esc

Printer-friendly Version

Interactive Discussion



Even though avalanche #1a was small, a significant powder cloud developed shortly after the release (Fig. 3). After the avalanche entered the open slope (37 s), plume formation stopped, accompanied by a visible decrease in velocity, and the powder cloud drifted to the up-hill looking right side (47 s) due to the prevailing wind, revealing the until then obscured dense core (57 s). After that a rapid cooling of the surface of the dense core could be observed (from pink colors at 57 s to orange at 77 s).

The IRT video of avalanche #2 (Fig. 5) is of special interest since a distinct acceleration of the avalanche can be observed as it approaches the open slope below the rock face (33 s). This can be explained by the entrainment of mass of the secondary release (42 s). The powder cloud shows higher temperatures than during the first phase (50 s) and the eroded surface becomes visible after the powder cloud drifts aside (56–82 s).

### 4.1.2 Surface temperature distribution

The IRT camera images acquired shortly after the avalanches stopped (Fig. 6) allowed to identify exposed deep, and thus warmer, layers in the release and along the path as well as in the deposited snow. In Fig. 6b the secondary release, below the steep rock part, showed a much deeper erosion in the, looking up-hill, left corner. In the lower part of the track erosion was spatially rather homogenous for all avalanches.

Lateral IRT surface temperature transects in the deposition area of avalanche #1 and #2 (black lines in Fig. 6) revealed that the warmest part of the avalanche is located in the center and therefore in its dense core (Fig. 7a and c). In both cases a distinct difference in surface temperature of multiple degree Celsius between undisturbed snow cover and warmer core of the avalanche is evident. Figure 7b shows lateral profiles (L1 and L2 in Fig. 6b) along the path of avalanche and allowed to differentiate between undisturbed snow cover, the deposits of a fluidized layer that formed at the lookers-left (South) side of avalanche #2 and the dense core.

### 4.1.3 Internal temperature distribution of deposits

The observed maximum temperatures in the dense core area did not only exist on the surface in lateral extension (Fig. 7) but also vertically in the deposits. This could be measured for both avalanches for which lateral investigations were conducted. Figure 8 shows the lateral temperature measurements conducted in the deposition zone of avalanche #2 and #3. Measurement  $P_{\text{depo}}$ , corresponding to 0 m, was located in the middle of the deposition and marked the position of the full snow profile in the deposits (Fig. 2). Temperature measurement locations R and L were leading laterally from the center to the, looking uphill, right and left side of the avalanche deposits. Furthermore, the top of the avalanche deposits (solid line), the bottom of the deposits (dashed line) and the terrain (pointed line) are indicated. For better distinction the area of the undisturbed snow cover is additionally indicated by softened colors. Even though the transect shown in Fig. 8a only represents one half of the avalanche deposits from avalanche #2, the extent of the dense core (area between solid and dashed line) could clearly be observed in the measured snow temperature. Similar measurements were recorded for avalanche #3 where again the highest temperatures were recorded in the center of the deposits (Fig. 8b) with decreasing values towards the side of the deposits.

### 4.2 Thermal energy sources

To explain the observed increased snow temperatures in the deposits of the investigated avalanches and to assign and order of magnitude estimation of the sources of thermal energy, we partitioned the total warming into (i) warming due to entrainment of snow and (ii) friction. Other potential sources of thermal energy, e.g. entrainment of air or adiabatic warming, were not considered in this calculation since their influence on the temperature of the dense core were estimated as negligibly small and in the presented work.

Title Page

Abstract

Introduction

Conclusions

References

Tables

Figures



Back

Close

Full Screen / Esc

Printer-friendly Version

Interactive Discussion



## 4.2.1 Entrainment

The snow profiles (see locations in Fig. 2) enabled a quantification of the properties of the released and entrained snow. Figure 9 shows snow temperature profiles in the center of the deposition zone  $T_{P_{\text{depo}}}$  (solid violet line) and compares them to measurements conducted in the release zone  $T_{P_{\text{release}}}$  (blue line), along the path in the undisturbed snow  $T_{P_{\text{track}}}$  (orange) and the undisturbed snow cover in the run out zone  $T_{P_{\text{runout}}}$  (gray). Comparing  $T_{P_{\text{depo}}}$  and  $T_{P_{\text{release}}}$  reveals that a significant warming took place.

Depth-averaging the deposition profile (violet line) yielded a snow temperature of  $-6.8^{\circ}\text{C}$  for avalanche #2 and  $-4.1^{\circ}\text{C}$  for avalanche #3. Temperature values from the upper and lowermost layers were excluded from the calculations because of adaption of the temperature with the surrounding air and undisturbed snow cover (gray areas in Fig. 9). Averaging, both spatially and vertically, the temperature for the snow that was released and entrained along the track results in  $-8.7$  and  $-5.8^{\circ}\text{C}$  for the two avalanches (Table 2). This resulted in a difference in snow temperature between entrained and deposited snow of  $\Delta T$  1.9 and  $1.7^{\circ}\text{C}$ , respectively. The temperature of the released and entrained snow could therefore not be the exclusive source of thermal energy.

## 4.2.2 Friction

The increase in temperature due to friction was calculated by assuming that all potential energy is transformed to heat. Starting with potential energy

$$E_{\text{pot}} = m g h, \quad (1)$$

where  $m$  is the mass,  $g$  is the gravitational acceleration ( $9.81 \text{ m s}^{-2}$ ) and  $h$  is the difference in elevation, we equated  $E_{\text{pot}}$  to the thermal energy  $E_{\text{therm}}$  resulting in

$$E_{\text{pot}} = m g h = E_{\text{therm}} = m c_p \Delta T, \quad (2)$$

Title Page

Abstract

Introduction

Conclusions

References

Tables

Figures



Back

Close

Full Screen / Esc

Printer-friendly Version

Interactive Discussion



where  $m$  is the mass,  $c_p$  is the specific heat capacity of snow ( $2116 \text{ J kg}^{-1} \text{ K}^{-1}$ ) and  $\Delta T$  is the change in snow temperature. Solving for  $\Delta T$  resulted in

$$\Delta T_{\text{friction}} = \frac{gh}{c_p}. \quad (3)$$

Note that  $m$  can be dropped if the mass is not assumed to change along the path (i.e. no erosion or deposition takes place). Calculating for an elevation drop of 300 m, corresponding to the slope below the rock face until the run out zone, resulted in an increase in temperature due to friction of approximately  $1.5^\circ\text{C}$ .

The calculated  $\Delta T_{\text{friction}}$  can be seen as a maximum value in our order of magnitude estimation since in nature not all mass is released and entrained at the maximum elevation  $h$ . Furthermore, lateral temperature gradients in the deposition area are not taken into account.

## 5 Discussion

It has been noted in other studies (Vera et al., 2012) that potential sources of thermal energy in snow avalanches are friction processes or entrainment of snow with differing temperatures. Our results confirm that for the investigated avalanches the thermal energy increase due to friction is mainly depending on the elevation drop of the avalanche and thus a rather constant value (for a specific avalanche path and typology). The basic calculation does not take changes in mass into account. Yet, it is well known that avalanches can significantly increase their mass along the path via entrainment (Sovilla, 2004). Therefore, the calculated value of  $0.5^\circ\text{C}$  per 100 altitudinal meters has to be adapted to consider the actual mass that enters the avalanche at a certain point along the track. For dry and cold snow avalanches far away from the melting point, the warming due to friction alone is therefore not expected to have a substantial influence on flow dynamics. Yet, if the overall avalanche temperature is already close to the critical temperature threshold of  $-1^\circ\text{C}$  (Steinkogler et al., 2014) the warming by frictional

## Thermal energy in dry snow avalanches

W. Steinkogler et al.

Title Page

Abstract

Introduction

Conclusions

References

Tables

Figures



Back

Close

Full Screen / Esc

Printer-friendly Version

Interactive Discussion



processes can cause drastic changes of the granular structure inside the avalanche and consequently affect flow behavior.

Contrary, the warming due to entrainment is very specific to the individual avalanche and can vary significantly depending on the erosion depth as shown in the profiles along the avalanche track (Fig. 9) and the IRT pictures (Fig. 6). The alpine snow cover typically shows a positive temperature gradient towards the ground (Armstrong and Brun, 2008). Except for areas with permanent permafrost the temperature at the soil–snow interface can be assumed to be approximately 0 °C if there has been a significant snow cover for several weeks. Consequently, the erosion of deeper snow layers leads to warmer snow temperatures. Also altitudinal changes of snow temperature along the slope have been proven to be quite variable and directly influence flow dynamics (Steinkogler et al., 2013).

Our temperature measurements on the surface (Fig. 7) and in depth (Fig. 8) of the deposition zone indicate that the highest temperatures are located in the dense core of the avalanche. The interface between the bottom of the avalanche deposits and the subjacent undisturbed snow cover featured a very clear and sharp transition (violet lines in Fig. 9). The shape of the temperature curve indicates the warmest temperatures in the lower parts of the deposits profile (–40 to –80 cm and –120 to –190 cm for avalanches #2 and #3, respectively) and close to the sliding surface. This would support the expectation of the most pronounced friction at the bottom of the flow, typical for this kind of avalanche. Unfortunately, a cooling of the lowest deposition layers to the temperature of the subjacent undisturbed snow cover has to be expected and thus prevents a definite conclusion on this observation. The upper part of the temperature profiles resemble more the shape of a plug-like flow. Also, whether the temperature variations in the upper part of the deposition profile between 0 and –100 cm of avalanche #3 (violet line in Fig. 9) are a result of a mixture of broken parts of the eroded snow cover, with varying temperatures, and formed granules could not be fully answered. Yet, granules embedded in fine grained snow were still clearly observable in this area of the deposition.

## Thermal energy in dry snow avalanches

W. Steinkogler et al.

Title Page

Abstract

Introduction

Conclusions

References

Tables

Figures



Back

Close

Full Screen / Esc

Printer-friendly Version

Interactive Discussion



**Thermal energy in  
dry snow avalanches**

W. Steinkogler et al.

Title Page

Abstract

Introduction

Conclusions

References

Tables

Figures



Back

Close

Full Screen / Esc

Printer-friendly Version

Interactive Discussion



It is without question that reaching the deposits after an avalanche release to measure the snow surface temperature with traditional methods, e.g. thermometers, takes too long and the surface as well as the upper most layers would have changed their temperature already. It could be observed in the video of avalanche #1 (see Supplement) that right after the dense core stopped it started to cool. In all those cases for which a real-time measurement is necessary IRT technology provides a valuable addition to traditional measurements. Even though in our study we only applied the IRT camera in a qualitative way, the presented basic verification (Fig. 4) with manually measured snow surface temperatures showed a fairly good agreement with an accuracy of about  $\pm 1^\circ\text{C}$ . Although further investigations are necessary to define whether absolute values of surface temperature can be acquired without significant uncertainties, the relative accuracy of the IRT cameras are usually high, around  $0.05^\circ\text{C}$  in our case as specified by the manufacturer. This facilitates to track relative changes in temperatures even if the absolute value might not be accurate.

Recently IRT was mainly tested and evaluated for snow profile applications at short distances (Schirmer and Jamieson, 2014). Possible influences of the large distances between camera and avalanches, viewing angle, liquid water content in snow or at its surface (Snyder et al., 1998) and surface roughness of the deposits (Mushkin et al., 2007; Danilina et al., 2006) demand detailed studies. In general, low signal attenuation can be expected for (peak) winter month atmospheres, especially for clear sky conditions, due to relatively low humidity levels.

Dozier and Warren (1982) investigated the effect of viewing angle on the infrared brightness temperature of snow and found differences of up to  $3^\circ\text{C}$ . Similar values have been found by Hori et al. (2013), yet they concluded that for viewing angles less than  $40^\circ$  from the nadir the error in temperature is less than  $-0.8^\circ\text{C}$ . The effect of moisture has been studied extensively (Wu et al., 2009, and references therein), basically concluding that the presence of water causes a strong absorbance and consequently a decrease in reflectance in the near-infrared spectra of soils.

## Thermal energy in dry snow avalanches

W. Steinkogler et al.

Title Page

Abstract

Introduction

Conclusions

References

Tables

Figures



Back

Close

Full Screen / Esc

Printer-friendly Version

Interactive Discussion



An effect that still illustrates challenges for the interpretation of IRT images is due to the roughness of the investigated surface (Wu et al., 2009). In most studies the assumption that the scene elements are isothermal, smooth and homogenous is used (Danilina et al., 2006). Consequently supposing that the object of interest is Lambertian, i.e. behaves as a perfect diffuser and emits and reflects radiation isotropically. Mushkin et al. (2007) observed that the effective emissivity spectra of rough surfaces are different from those of perfectly smooth surfaces of the same composition due to multiple scattering among roughness elements. Yet, they only found an up to 3% reduction in the spectral contrast due to sub-pixel surface roughness variations.

Also whether the surface temperature, and possibly even the composition, of the aerosol mixture of the powder cloud can be measured is an open question. Visualization of air flows on the qualitative level is common practice for various applications (Narayanan et al., 2003; Carlomagno and Cardone, 2010) and, as presented in this study, provides impressive footage of powder snow avalanches. Usually a tracer is injected into the flow field. In our case the tracer is already present by snow particles of the entrained snow which are transported into the powder cloud. Similar concepts as applied for satellite remote sensing of high-level clouds, such as cirrus (Fu et al., 1998), might be transferable to avalanche powder clouds.

A possible further application of IRT could be the differentiation of flow regimes in the deposition area. As shown earlier the warmest part of an avalanche is located in the dense core, e.g. center (red and pink) of avalanche #2 in Fig. 6b, whereas layers with less mass or where less friction occurred are cooler (yellow and orange areas in Fig. 6b). Especially the lookers-left (South) side of the deposition in Fig. 6b appears to be the deposits of a fluidized layer. The IRT observations are in agreement with the field observation criteria for fluidized layers as described by Issler et al. (2008): (1) rapid decrease of deposit thickness, (2) snowballs of various sizes embedded in a matrix of compacted fine-grained snow, (3) large snowballs lying on top of the deposit and (4) fewer snowballs per unit area than on the dense deposit.

---

**Thermal energy in  
dry snow avalanches**

---

W. Steinkogler et al.

---

[Title Page](#)[Abstract](#)[Introduction](#)[Conclusions](#)[References](#)[Tables](#)[Figures](#)[Back](#)[Close](#)[Full Screen / Esc](#)[Printer-friendly Version](#)[Interactive Discussion](#)

Deposits from the powder cloud have consistently lower temperatures than the warm dense core despite the fact that the powder cloud (at least from one avalanche) traveled as far downhill as the dense core. Two distinct processes may contribute to this fact: (i) a preferential ejection of colder and lighter surface snow layers already initiates suspension with colder snow while the dense core may have a higher fraction of snow from lower layers in the profile and therefore with a higher temperature. (ii) The particle concentration in the suspension layer is low and therefore molecular dissipation of kinetic energy and exchange of sensible and latent heat happens largely between air and snow and not between snow and snow particles as in the dense core. This leads to a rapid adoption of temperatures close to the air temperature for the suspended snow.

Furthermore, the IRT results can be qualitatively interpreted in a similar way as a laser scan to identify areas where deeper or shallower erosion occurred, e.g. see step-down entrainment below the rock face for avalanche #2 (Fig. 6b). For this avalanche we exemplarily calculated the release mass solely by using information from the IRT pictures and manually measured snow profiles in the release. Therefore, the IRT picture was georeferenced in a GIS software and shallower and deeper release layers were identified. The (IRT) surface temperature of these layers were combined with the snow height of the corresponding temperature in the conducted snow profile in the release. This resulted in a calculated release mass of 457 t which is similar to the mass measured with the terrestrial laser scan (502 t). This depicts a rough yet quick and efficient method to estimate the release mass of an avalanche. As shown in this study, the release and entrainment depth does not only define the overall mass of snow but equally important its temperature. IRT pictures and videos provide an intuitive and easy to acquire measure to identify these relevant erosion processes (Fig. 6).

## 6 Conclusions

We conducted full-scale avalanche experiments at the Flüelapass field site above Davos (Switzerland) to investigate the distribution of snow temperatures in avalanche

deposits and identify the sources of thermal energy in dry avalanches. A further goal was to test the usability of infrared radiation thermography (IRT) in this context.

For the investigated similar avalanches the temperature increase due to friction was mainly dependent on the elevation the avalanche dropped. The contribution to the total temperature increase by erosion processes was shown to be quite variable, depending on the release depth and snow temperatures of the entrained snow. The warmest temperatures were observed in the center of the avalanche deposits and thus represented the dense core of the flowing avalanche.

The IRT camera allowed to observe the avalanche phenomenon “with different eyes” and provides a lot of potential for more detailed research in the field of avalanche dynamics, both quantitative and qualitative. It is still necessary to further verify the measurements and define to which extent absolute snow surface temperatures can be measured. Then, the spatial distribution of surface temperatures can help in the interpolation of profile temperatures measured by hand.

Our results allow for a more comprehensive understanding of snow temperatures in avalanche flow and their consequences on flow regimes. This information can directly be used to verify and enhance the performance of avalanche dynamics models and is thus of great interest for practitioners.

**The Supplement related to this article is available online at  
doi:10.5194/tcd-8-5793-2014-supplement.**

*Acknowledgements.* Funding for this research has been provided through the Interreg project STRADA by the following partners: Amt für Wald Graubünden, Etat du Valais, ARPA Lombardia, ARPA Piemonte, Valle d’Aosta, Regione Lombardia. The authors would like to thank all the people who helped gathering the data during the field experiments. Thanks to Vali Meier from the SOS Service Jakobshorn (Davos) and his team for the great support.

Thermal energy in dry snow avalanches

W. Steinkogler et al.

Title Page	
Abstract	Introduction
Conclusions	References
Tables	Figures
◀	▶
◀	▶
Back	Close
Full Screen / Esc	
Printer-friendly Version	
Interactive Discussion	



## References

- Armstrong, R. L. and Brun, E.: Snow and Climate: Physical Processes, Surface Energy Exchange and Modeling, Cambridge University Press, Cambridge, UK, 222 pp., 2008. 5806
- Bartelt, P., Bühler, Y., Buser, O., Christen, M., and Meier, L.: Modeling mass-dependent flow regime transitions to predict the stopping and depositional behavior of snow avalanches, *J. Geophys. Res.*, 117, doi:10.1029/2010JF001957, online first, 2012. 5795
- Bates, B., Ancey, C., and Busson, J.: Visualization of the internal flow properties and the material exchange interface in an entraining viscous Newtonian gravity current, *Environ. Fluid Mech.*, 14, 501–518, 2014. 5795
- Brenning, A., Gruber, S., and Hoelzle, M.: Sampling and statistical analyses of BTS measurements, *Permafrost Periglac.*, 16, 383–393, 2005. 5797
- Carlomagno, G. and Cardone, G.: Infrared thermography for convective heat transfer measurements, *Exp. Fluids*, 49, 1187–1218, doi:10.1007/s00348-010-0912-2, 2010. 5808
- Danilina, I., Mushkin, A., Gillespie, A., O’Neal, M., Pietro, L., and Balick, L.: Roughness effects on sub-pixel radiant temperatures in knetically isothermal surfaces, in: RAQRS II: 2nd International Symposium on Recent Advances in Quantitative Remote Sensing, 25–29 September 2006, Torrent (Valencia), Spain, available at: [gis.ess.washington.edu/keck/raqrs\\_files/RAQRS\\_II\\_Danilina\\_etal.pdf](http://gis.ess.washington.edu/keck/raqrs_files/RAQRS_II_Danilina_etal.pdf), 2006. 5807, 5808
- Dozier, J. and Warren, S. G.: Effect of viewing angle on the infrared brightness temperature of snow, *Water Resour. Res.*, 18, 1424–1434, doi:10.1029/WR018i005p01424, 1982. 5807
- Fierz, C., Armstrong, R., Durand, Y., Etchevers, P., Greene, E., McClung, D., Nishimura, K., Satyawali, P., and Sokratov, S.: The international classification for seasonal snow on the ground, IHP-VII Technical Documents in Hydrology, UNESCO-IHP, Paris, 83, 2009. 5797
- Fu, Q., Yang, P., and Sun, W.: An accurate parameterization of the infrared radiative properties of cirrus clouds for climate models, *J. Climate*, 11, 2223–2237, 1998. 5808
- Gauer, P., Issler, D., Lied, K., Kristensen, K., and Sandersen, F.: On snow avalanche flow regimes: inferences from observations and measurements, in: Proceedings, International Snow Science Workshop ISSW 21–27 September 2008, Whistler, Canada, 717–723, 2008. 5794
- Hori, M., Aoki, T., Tanikawa, T., Hachikubo, A., Sugiura, K., Kuchiki, K., and Niwano, M.: Modeling angular-dependent spectral emissivity of snow and ice in the thermal infrared atmospheric window, *Appl. Optics*, 52, 7243–7255, doi:10.1364/AO.52.007243, 2013. 5807

## Thermal energy in dry snow avalanches

W. Steinkogler et al.

Title Page

Abstract

Introduction

Conclusions

References

Tables

Figures



Back

Close

Full Screen / Esc

Printer-friendly Version

Interactive Discussion



## Thermal energy in dry snow avalanches

W. Steinkogler et al.

Title Page

Abstract

Introduction

Conclusions

References

Tables

Figures

◀

▶

◀

▶

Back

Close

Full Screen / Esc

Printer-friendly Version

Interactive Discussion



- Issler, D., Errera, A., Priano, S., Gubler, H., Teufen, B., and Krummenacher, B.: Inferences on flow mechanisms from snow avalanche deposits, *Ann. Glaciol.*, 49, 187–192, 2008. 5808
- Lewkowicz, A. G. and Ednie, M.: Probability mapping of mountain permafrost using the BTS method, Wolf Creek, Yukon Territory, Canada, *Permafrost Periglac.*, 15, 67–80, 2004. 5797
- 5 Meola, C. and Carlomagno, G. M.: Recent advances in the use of infrared thermography, *Measurement Science and Technology*, 15, R27, doi:10.1088/0957-0233/15/9/R01, 2004. 5795
- Mushkin, A., Danilina, I., Gillespie, A. R., Balick, L. K., and McCabe, M. F.: Roughness effects on thermal-infrared emissivities estimated from remotely sensed images, in: *Remote Sensing for Environmental Monitoring, GIS Applications, and Geology VII*, 67492V, doi:10.1117/12.738125 2007. 5807, 5808
- 10 Naaim, M., Durand, Y., Eckert, N., and Chambon, G.: Dense avalanche friction coefficients: influence of physical properties of snow, *J. Glaciol.*, 59, 771–782, doi:10.3189/2013JoG12J205, 2013. 5794, 5795
- Narayanan, V., Page, R., and Seyed-Yagoobi, J.: Visualization of air flow using infrared thermography, *Exp. Fluids*, 34, 275–284, 2003. 5808
- 15 Schirmer, M. and Jamieson, B.: Limitations of using a thermal imager for snow pit temperatures, *The Cryosphere*, 8, 387–394, doi:10.5194/tc-8-387-2014, 2014. 5795, 5796, 5807
- Shea, C. and Jamieson, B.: Some fundamentals of handheld snow surface thermography, *The Cryosphere*, 5, 55–66, doi:10.5194/tc-5-55-2011, 2011. 5795
- 20 Shea, C., Jamieson, B., and Birkeland, K. W.: Use of a thermal imager for snow pit temperatures, *The Cryosphere*, 6, 287–299, doi:10.5194/tc-6-287-2012, 2012. 5795
- Snyder, W. C., Wan, Z., Zhang, Y., and Feng, Y.-Z.: Classification-based emissivity for land surface temperature measurement from space, *Int. J. Remote Sens.*, 19, 2753–2774, doi:10.1080/014311698214497, 1998. 5795, 5807
- 25 Sovilla, B.: Field experiments and numerical modelling of mass entrainment and deposition processes in snow avalanches, Dissertation no. 15462, Swiss Federal Institute of Technology, Zürich, 2004. 5805
- Sovilla, B., Margreth, S., and Bartelt, P.: On snow entrainment in avalanche dynamics calculations, *Cold Reg. Sci. Technol.*, 47, 69–79, doi:10.1016/j.coldregions.2006.08.012, 2007. 5795
- 30 Steinkogler, W., Sovilla, B., and Lehning, M.: Influence of snow cover properties on avalanche dynamics, *Cold Reg. Sci. Technol.*, 97, 121–131, doi:10.1016/j.coldregions.2013.10.002, 2013. 5795, 5806

Steinkogler, W., Gaume, J., Löwe, H., Sovilla, B., and Lehning, M.: Granulation of snow: from tumbler experiments to discrete element simulations, *J. Geophys. Res.*, in review, 2014. 5795, 5805

Vera, C., Feistl, T., Steinkogler, W., Buser, O., and Bartelt, P.: Thermal Temperature in Avalanche Flow, in *Proceedings, International Snow Science Workshop ISSW 16–21 September 2012, Anchorage, Alaska*, 32–37, 2012. 5805

Wu, C.-Y., Jacobson, A. R., Laba, M., and Baveye, P. C.: Accounting for surface roughness effects in the near-infrared reflectance sensing of soils, *Geoderma*, 152, 171–180, doi:10.1016/j.geoderma.2009.06.002, 2009. 5807, 5808

TCD

8, 5793–5824, 2014

## Thermal energy in dry snow avalanches

W. Steinkogler et al.

Title Page

Abstract

Introduction

Conclusions

References

Tables

Figures



Back

Close

Full Screen / Esc

Printer-friendly Version

Interactive Discussion



## Thermal energy in dry snow avalanches

W. Steinkogler et al.

**Table 1.** Summary of measurements for the investigated avalanches. \* indicate that erosion and deposition depths were too small.

Avalanche	#1a	#2	#3
Date	23 Jan 2013	5 Feb 2013	31 Jan 2014
IRT camera model	hr 384 sl	hr 384 sl	HD 980 s
Terrestrial laser scan	no	partly	yes
Snow profiles lateral	–*	yes	yes
Snow profiles track	–*	yes	yes
IRT video	yes	yes	no
IRT pictures	yes	yes	yes
Released mass (t)	–	502	818
Entrained mass (t)	–	1857	1302
Deposited mass (t)	–	2359	2120

Title Page

Abstract

Introduction

Conclusions

References

Tables

Figures

◀

▶

◀

▶

Back

Close

Full Screen / Esc

Printer-friendly Version

Interactive Discussion



## Thermal energy in dry snow avalanches

W. Steinkogler et al.

**Table 2.** Depth averaged temperatures of release ( $\overline{T_{P_{\text{release}}}}$ ), track ( $\overline{T_{P_{\text{track}}}}$ ) and deposition profile ( $\overline{T_{P_{\text{depo}}}}$ ) with the corresponding release and erosion depths (in brackets). The mean temperature  $\text{mean}(T) = \overline{T_{P_{\text{cornice}}} + \overline{T_{P_{\text{release}}} + \overline{T_{P_{\text{track}}}}$  in comparison to  $\overline{T_{P_{\text{depo}}}}$  results in the temperature difference between released and deposited snow  $\Delta T$  which can not be explained by the entrained snow.

Avalanche	#2	#3
$\overline{T_{P_{\text{cornice}}}}$	–	–5.3 °C (1.05 m)
$\overline{T_{P_{\text{release}}}}$	–8.6 °C (1.03 m)	–6.3 °C (1.75 m)
$\overline{T_{P_{\text{track}}}}$	–8.7 °C (0.37 m)	–5.8 °C (0.3 m)
$\text{mean}(T)$	–8.7 °C	–5.8 °C
$\overline{T_{P_{\text{depo}}}}$	–6.8 °C (0.9 m)	–4.1 °C (1.95 m)
$\Delta T$	1.9 °C	1.7 °C

Title Page

Abstract

Introduction

Conclusions

References

Tables

Figures

◀

▶

◀

▶

Back

Close

Full Screen / Esc

Printer-friendly Version

Interactive Discussion



## Thermal energy in dry snow avalanches

W. Steinkogler et al.

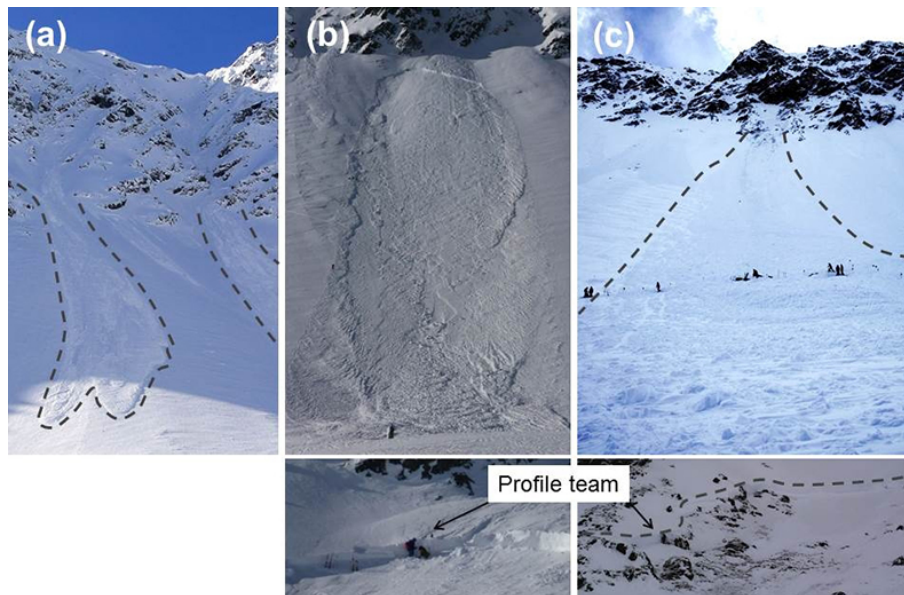


**Figure 1.** Avalanches at the Flüelapass field site released by artificial triggering of the cornices on the ridge. Avalanche #1a and #1b **(a)** were released on 23 January 2013, #2 **(b)** on 05 February 2013 and #3 **(c)** on 31 January 2014. Note the significant step-down and entrainment of deeper layers below the rock face for **(b)** avalanche #2 and **(c)** avalanche #3.

[Title Page](#)[Abstract](#)[Introduction](#)[Conclusions](#)[References](#)[Tables](#)[Figures](#)[I◀](#)[▶I](#)[◀](#)[▶](#)[Back](#)[Close](#)[Full Screen / Esc](#)[Printer-friendly Version](#)[Interactive Discussion](#)

Thermal energy in  
dry snow avalanches

W. Steinkogler et al.

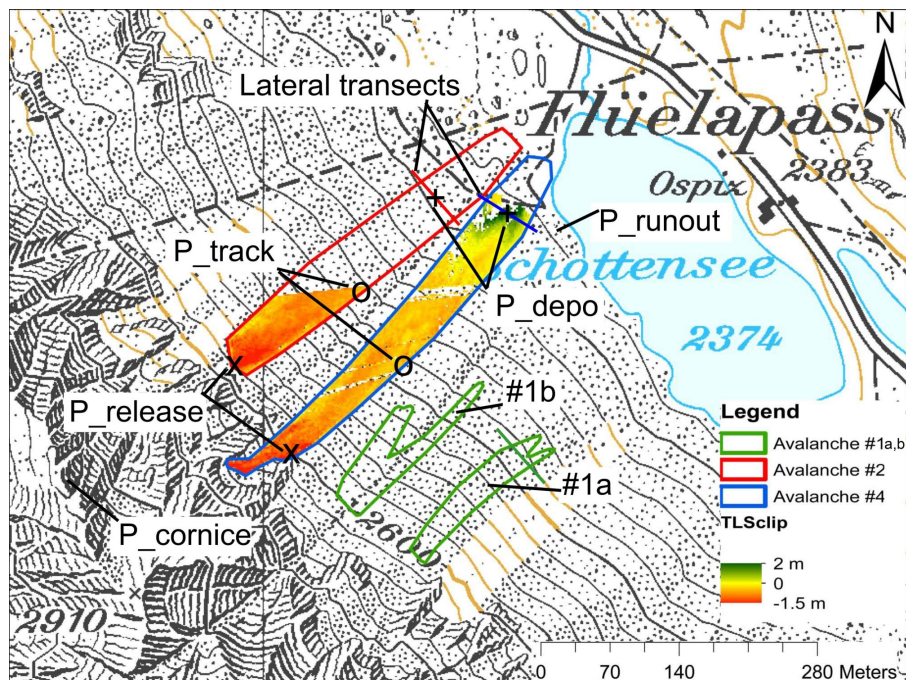


**Figure 2.** Flüelapass field site close to Davos (Switzerland). Outlines of avalanche #1a and #1b (green), #2 (red) and #3 (blue). The colorbar shows differences between terrestrial laser scans before and after the individual avalanches.  $P_{\text{release}}$  and  $P_{\text{track}}$  indicate locations of snow profile in the release and along the path, respectively. Red and blue lines indicate positions of lateral investigations and deposition snow profile  $P_{\text{depo}}$ .

Title Page

Abstract

Introduction

Conclusions

References

Tables

Figures

◀

▶

◀

▶

Back

Close

Full Screen / Esc

Printer-friendly Version

Interactive Discussion



## Thermal energy in dry snow avalanches

W. Steinkogler et al.

Title Page

Abstract

Introduction

Conclusions

References

Tables

Figures



Back

Close

Full Screen / Esc

Printer-friendly Version

Interactive Discussion

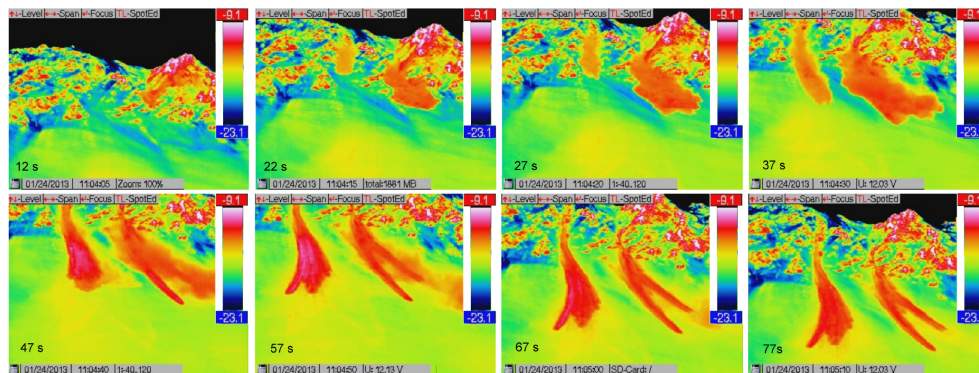


**Figure 3.** Screenshot of IRT camera videos for avalanche #1a and #1b. The first picture was taken 12 s after the avalanche released.

## Thermal energy in dry snow avalanches

W. Steinkogler et al.

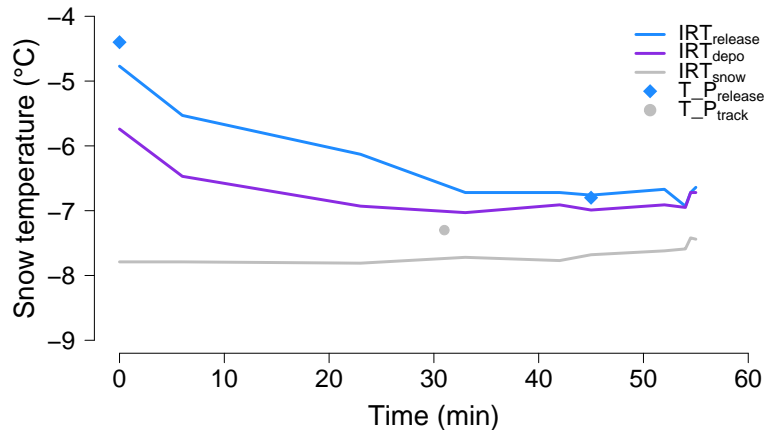


**Figure 4.** Temporal evolution and comparison of snow temperatures using a IRT camera and manually measured data. Solid lines represent regular IRT measurements in the release ( $IRT_{\text{release}}$ ), the deposition area ( $IRT_{\text{depo}}$ ) and the undisturbed snow cover ( $IRT_{\text{snow}}$ ) which are compared to manual measurements at the profile locations ( $T_{\text{P}}_{\text{release}}$  and  $T_{\text{P}}_{\text{track}}$ ).

Title Page

Abstract

Introduction

Conclusions

References

Tables

Figures

◀

▶

◀

▶

Back

Close

Full Screen / Esc

Printer-friendly Version

Interactive Discussion



## TCD

8, 5793–5824, 2014

Thermal energy in  
dry snow avalanches

W. Steinkogler et al.

Title Page

Abstract

Introduction

Conclusions

References

Tables

Figures



Back

Close

Full Screen / Esc

Printer-friendly Version

Interactive Discussion

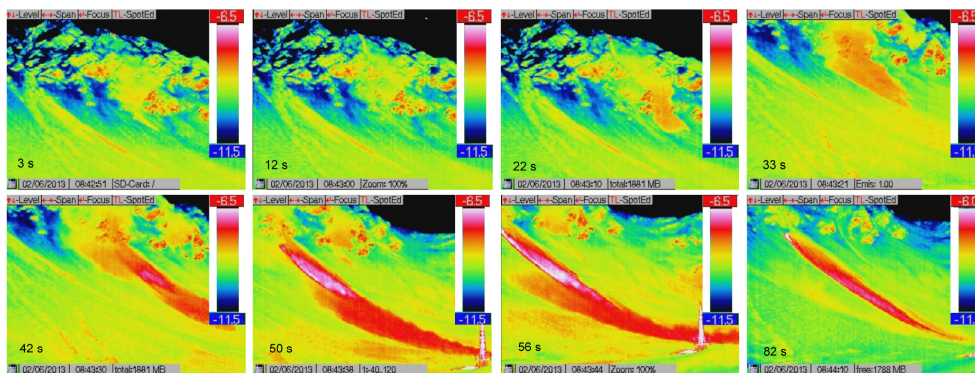


**Figure 5.** Screenshot of IRT camera videos for avalanche #2. The first picture was taken 3 s after the avalanche released. Note that the temperature scale was changed by  $0.5^{\circ}\text{C}$  for the last shown image (82 s).

Thermal energy in  
dry snow avalanches

W. Steinkogler et al.

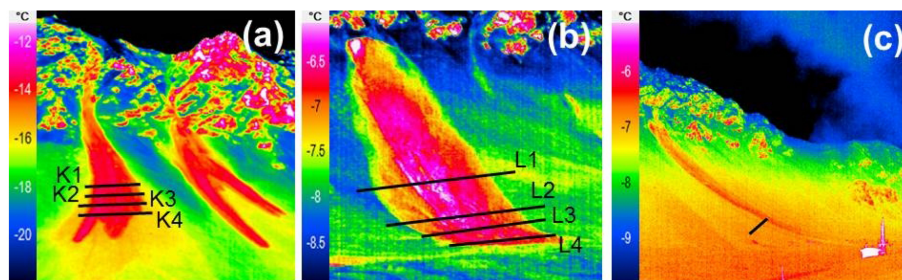


**Figure 6.** IRT camera images for avalanches **(a)** #1a and #1b, **(b)** #2 and **(c)** #3. Note the different temperature scales amongst the avalanches. Black lines indicate positions of lateral snow temperature transects and profiles.

Title Page

Abstract

Introduction

Conclusions

References

Tables

Figures

◀

▶

◀

▶

Back

Close

Full Screen / Esc

Printer-friendly Version

Interactive Discussion



## Thermal energy in dry snow avalanches

W. Steinkogler et al.

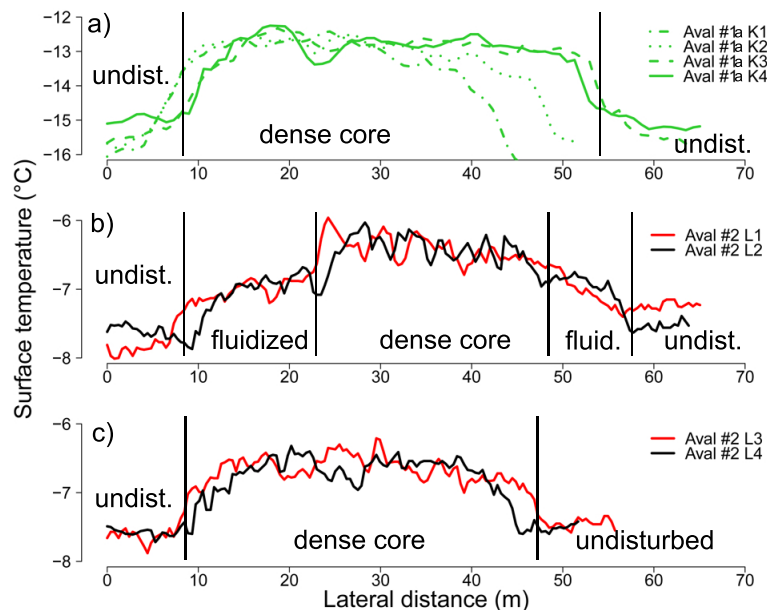


**Figure 7.** Snow surface temperatures acquired with IRT along lateral transects for avalanche #1 (a) and in the path (b) and the deposition area (c) of avalanche #2. Extent of undisturbed snow cover, area of fluidized layer and dense core are indicated.

Title Page

Abstract

Introduction

Conclusions

References

Tables

Figures

◀

▶

◀

▶

Back

Close

Full Screen / Esc

Printer-friendly Version

Interactive Discussion



Thermal energy in  
dry snow avalanches

W. Steinkogler et al.

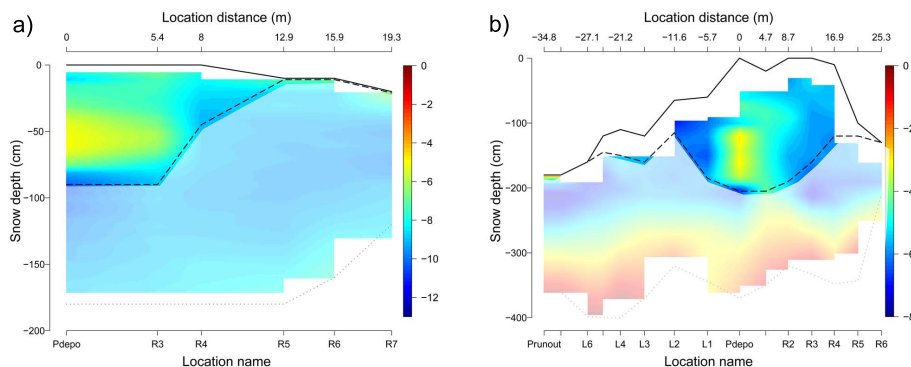


**Figure 8.** Lateral snow temperature profiles in the avalanche deposits of **(a)** avalanche #2 and **(b)** avalanche #3.  $P_{\text{depo}}$  and 0 m indicate the center of deposits and the index L and R represent left and right, looking uphill, measurement locations towards the lateral sides of the avalanches. Lines indicate the top of the avalanche deposit or snow cover (solid), bottom of avalanche deposit (dashed) and bottom of snow cover (pointed). Colors of undisturbed snow cover were softened for better distinction with avalanche deposits.

Title Page

Abstract

Introduction

Conclusions

References

Tables

Figures



Back

Close

Full Screen / Esc

Printer-friendly Version

Interactive Discussion



## Thermal energy in dry snow avalanches

W. Steinkogler et al.

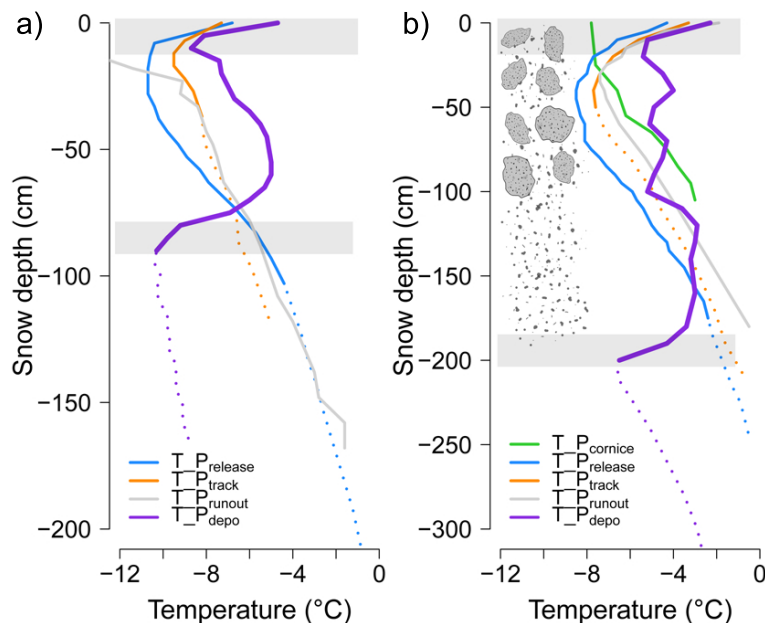


**Figure 9.** Snow temperature measurements conducted in the release zone ( $T_{P_{\text{release}}}$ ), along the path in the undisturbed snow ( $T_{P_{\text{track}}}$ ), in the undisturbed snow cover in the run out zone ( $T_{P_{\text{runout}}}$ ) and in the deposition zone ( $T_{P_{\text{depo}}}$ ) of (a) avalanche #2 and (b) avalanche #3. Release, entrainment and deposition depths are indicated by solid lines whereas the undisturbed snow cover is represented by pointed lines. Gray areas indicate parts of the temperature profiles that were neglected in the calculations because of expected changes in temperature over time due to the boundary conditions of the surface and the undisturbed snow cover. Composition of deposits (granules and fine grains) are indicated for avalanche #2.

Title Page

Abstract

Introduction

Conclusions

References

Tables

Figures

◀

▶

◀

▶

Back

Close

Full Screen / Esc

Printer-friendly Version

Interactive Discussion

